

Enhancing Representation in Radiography-Reports Foundation Model: A Granular Alignment Algorithm Using Masked Contrastive Learning

Weijian Huang^{1,2,3}, Hongyu Zhou⁴, Cheng Li¹, Hao Yang^{1,2,3}, Jiarun Liu^{1,2,3}, and Shanshan Wang^{1,2}

¹ Paul C. Lauterbur Research Center for Biomedical Imaging, Shenzhen Institute of Advanced Technology, Shenzhen, China

² Pengcheng Laboratory, Shenzhen, China

³ University of Chinese Academy of Sciences, Beijing, China

⁴ University of Hong Kong, Hong Kong, China

Sophiasswang@hotmail.com, ss.wang@siat.ac.cn

Abstract. Recently, multi-modal vision-language foundation models have gained significant attention in the medical field. While these models offer great opportunities, they still face a number of challenges, such as the requirement for fine-grained knowledge understanding in computer-aided diagnosis and capability of utilizing very limited or no task-specific labeled data in real-world clinical applications. In this study, we present MaCo, a novel multi-modal medical foundation model that explores masked contrastive learning to achieve granular alignment and zero-shot learning for a variety of medical imaging tasks. MaCo incorporates a correlation weighting mechanism to adjust the correlation between masked image patches and their corresponding reports, thereby enhancing the representation learning capabilities. We evaluate MaCo on six well-known open-source X-ray datasets, and the experimental results show it outperforms seven state-of-the-art approaches for classification, segmentation, and zero-shot phase grounding, demonstrating its great potential to promote a wide range of medical image analysis tasks.

Keywords: Multi-Modal Representation · Vision-Language Representation Learning · Medical Foundation Model

1 Introduction

Recent advances in machine learning have enabled automated diagnostic systems (ADS) to approach expert-level performance, making it feasible to use deep learning to improve the clinical workflow [1]. These ADS have proven effective in handling common clinical applications, such as disease diagnosis and lesion quantification, through the training of various machine learning models [1]. However, training separate models for specific applications from scratch can be computationally expensive and requires a considerable amount of manually annotated

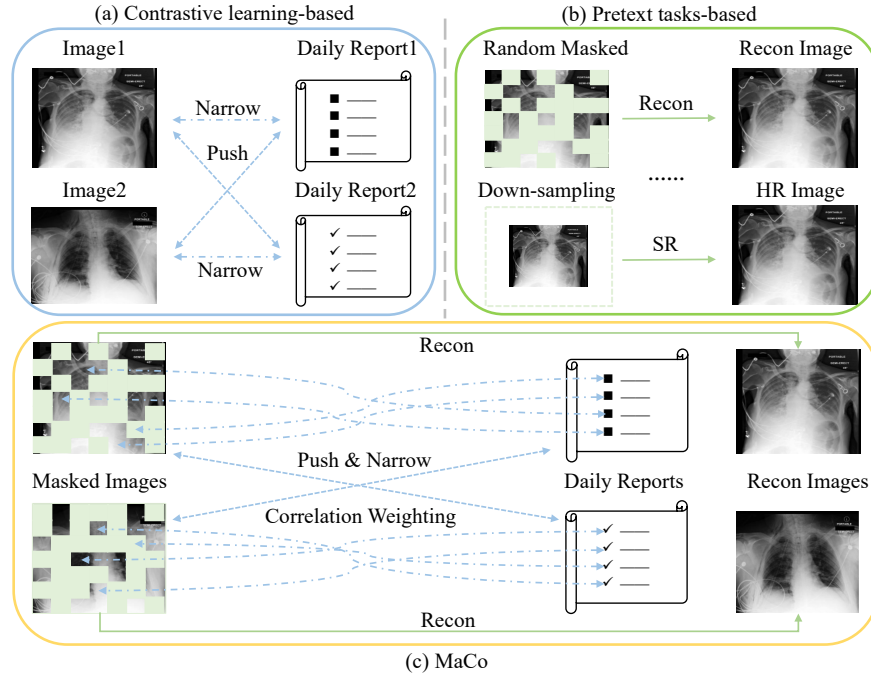


Fig. 1. The proposed MaCo framework. A novel masked contrast learning strategy is employed to leverage the advantages of both contrastive learning and pretext tasks simultaneously.

data, which fundamentally limits the development of medical applications [2]. As a result, there is an urgent need to explore alternative approaches that can improve the effectiveness of ADS training.

One promising approach to improve the effectiveness of ADS is to develop medical foundation models that can handle multiple clinical applications simultaneously and leverage pre-trained models to reduce the need for large annotated datasets [2]. These models can be trained on diverse and representative image-based datasets using self-supervised methods that do not require annotations, allowing them to learn robust and transferable feature representations that can be used across various tasks and domains [3]. By deploying simple task-based heads with well-learned feature representations obtained from the foundation model, such methods can achieve good performance in specific tasks without requiring that much of manual annotations compare to custom deep-learning training process [4]. This reduces the labeling burden on clinical experts and has better potential for clinical deployment. However, as these methods are gradually being adopted, the higher precision requirements in clinical deployment environments and the need for task generalization in open environments pose greater challenges for researchers.

Integrating expert knowledge with ADS has shown promising results as it combines human insight with feature distribution obtained through data-driven machine approaches [2, 5]. This approach has the potential to result in more reliable and intuitive results, making it a valuable tool for improving the performance of ADS. Coincidentally, radiology reports obtained from daily clinical examinations often contain rich information on healthcare history, imaging manifestations, and disease severity, making them suitable for providing human knowledge to the model. However, extracting meaningful information from these reports remains a pressing issue, as they are highly subjective, unstructured, and reliant on the individual style of the clinical physician. Achieving effective integration of these modalities remains in challenging.

Researchers have made efforts to effectively leverage expert knowledge from clinical reports, which can be broadly categorized into two branches. Some methods focus on improving radiological representations for down-stream tasks through fine-tuning. They carefully design self-supervised pretext tasks, such as using masked autoencoders (MAE) to obtain robust image representations [4], and then integrate them with the text branch to enhance the performance of down-stream fine-tuning tasks [6, 7]. On the other hand, some methods draw inspiration from contrastive learning [8], aligning the feature distributions of images and texts [2, 9, 10]). In addition to achieving comparable fine-tuning performance, they also acquire zero-shot capabilities to cope with the complex and diverse clinical environment. [11] has suggested that finding a better balance between these generative and discriminative methods could be beneficial, but such attempts have not yet been explored in the medical field.

In this paper, we focus on two key aspects when considering methods for medical vision-language foundation model. Firstly, we highlight the indispensability of fine-grained semantic understanding across the radiography and the clinical report. Given the intrinsic reliance on detailed descriptions in medical knowledge [2], attaining precise semantic comprehension represents a pivotal stride towards advancing precision medicine. Secondly, we advocate for the foundation model to exhibit a certain level of capability even under extreme conditions of limited annotations [1], where a scarcity of labeled data for down-stream tasks may prevail. This ensures the continued effectiveness of the foundation model, even in scenarios where no annotations are available for the task. We introduce a masked contrastive medical foundation model (MaCo) that aims to achieve granular alignment to enhance the feature representation. Our experimental results demonstrate the superiority of MaCo over all models with zero-shot learning in down-stream fine-tuning tasks. These findings underscore the potential of MaCo in reducing annotation costs in medical applications.

2 Related work

The expensive annotation has long been a persistent challenge in the field of medical. The primary approach to alleviate the annotation requirements in down-stream tasks is the utilization of pre-trained models. With the rapid advancement

of natural language models in recent years, there has been a growing focus on effectively integrating expert knowledge from clinical reports. In the following sections, this paper will explore relevant studies in the medical domain, specifically within the realm of self-supervised pretext task based and contrastive learning models. Emphasis will be placed on widely adopted techniques such as MAE and CLIP, along with their associated derivative methods.

2.1 Pretext tasks-based methods

The goal of pretext tasks-based methods is to construct image representations that are semantically meaningful that do not require downstream annotations [12,13]. These pretext tasks typically involve self-supervised learning, such as using randomly augmented images or training on downsampled images for super-resolution purposes. MAE [4] employs a random masking technique on image patches within the input data. Subsequently, a reconstruction decoder is utilized to recover the masked regions. By engaging in the reconstruction process, MAE is able to learn image features that can be subsequently utilized for down-stream tasks. Due to its simplicity and effectiveness, this method has gained considerable popularity among researchers, including the domain of medical image-text modeling. Drawing inspiration from MAE, [6] employ a masked mechanism in both the reports branch and the image branch of their models (MRM). They leverage the vision representation as a supplementary component to the text branch and enhance the feature representations through back-propagation optimization. Similar to MRM, [7] also employs masking in both the image and text encoders but adopts a more intricate approach to integrate and couple the features of the two modalities (M3AE).

Although the above methods have shown promising performance in downstream fine-tuning tasks, their zero-shot capability is hindered due to the modalities coupling. This limitation can restrict their task generalization, especially when dealing with unlabeled datasets.

2.2 Contrastive-learning-based methods

Contrastive-learning-based methods, on the other hand, has recently gained significant attention from researchers due to its unique zero-shot capability [14,15]. Contrastive learning aims to minimize the similarity distance between paired data points within a training batch while simultaneously maximizing the dissimilarity from other unpaired feature representations. By leveraging this approach, the trained model becomes proficient in differentiating between paired and unpaired images and texts, thereby acquiring the ability to generalize to unseen data samples, known as zero-shot capability [16].

[16] were pioneers in introducing the utilization of contrastive learning as a proxy task in the field of medicine. Their study effectively demonstrated the efficacy of contrastive learning within the medical domain. Building upon this foundation, [17] further investigated the impact of false negative samples on contrastive learning performance. [10] recognized the distinct language patterns

found in medical reports, prompting a redesign of the language model for medical Vision-Language Processing. [18] and [3] employed past radiology images and multi-view images, respectively, for joint training purposes. In more recent developments, [2] and [5] integrated a report filter to extract medical entities and employed a more complex modal fusion module to aggregate features, thereby achieving improved results. On the other side, to establish fine-grain representation between images and reports, [9] proposes a local fine-grained weighting mechanism. This mechanism calculates the similarity between each word and image patches, resulting in word-level responses. Similarly, [19] introduce the concept of multi-granularity alignment to explicitly learn the correspondence between fine-grained vision tokens and text tokens.

These methods have achieved comparable performance in down-stream fine-tuning tasks. More importantly, some methods such as BioViL and GLoRIA have demonstrated zero-shot capabilities, which greatly enhance the task generalization of medical models.

3 Methods

We introduce MaCo, a masked contrastive learning medical radiography-reports foundation model with zero-shot capability for down-stream tasks. The motivation behind MaCo is to leverage the advantages of both generative and discriminative learning methods to acquire enhanced semantic latent representations. We employ a masked autoencoder along with contrastive learning to facilitate learning on paired radiological images and medical reports. Additionally, we propose a correlation weighting mechanism that weights the contrastive loss based on the importance of sampled image patches. Fig. 2 illustrates the weighting mechanism, and specific details will be presented in the subsequent sections.

3.1 Radiography Mask-Auto-Encoding

To extract meaningful feature representations from input images, MaCo requires an vision encoder that maps the observed signal to a latent representation. Here, we adopt MAE proposed by [4] as our primary image representation extractor.

We divide the input image into regular, non-overlapping patches and randomly sample a subset of patches to remove the remaining ones. Once we have selected the subset of patches to use as input, our image encoder uses a vision transformer to generate the feature representations for each patch. The vision transformer applies self-attention mechanisms to the input patches, enabling it to model complex spatial relationships and capture long-range dependencies. The output of the image encoder is a set of feature representations, one for each input patch.

Let $v_{recon} \in \mathbb{R}^{B \times N \times C}$ denote the batch of embeddings for the masked reconstruction patches, and $g_{recon} \in \mathbb{R}^{B \times N \times C}$ denote the corresponding embeddings for the ground truth patches. Here, B , N , and C represent the batch size, the

number of sampled patches, and the dimension of the embeddings, respectively. We use a simple Mean-Square-Error as the reconstruction loss function:

$$\mathcal{L}_{mae} = (v_{recon} - g_{recon})^2 \quad (1)$$

3.2 Report Embedding

We adopt Bert [20], a classical natural language processing model that has achieved outstanding performance on a variety of language understanding tasks, to extract expert knowledge from clinical daily examination reports.

The clinical reports is processed by dividing them into multiple sentences, randomly selecting and shuffling the sentences is also considered in this step. Next, we use a wordpiece tokenizer to convert the preprocessed reports into a sequence of numerical tokens that can be processed by Bert. The wordpiece tokenizer breaks down each word into subword units and maps them to their corresponding numerical representations. This allows Bert to capture the meaning of the text at a more granular level, improving the quality of the sentence representations. Finally, we feed the sequence of numerical tokens into Bert to obtain sentence representations. These sentence representations capture the main ideas and themes from the clinicians hand writing reports and will be used to interact with image representations in the next section.

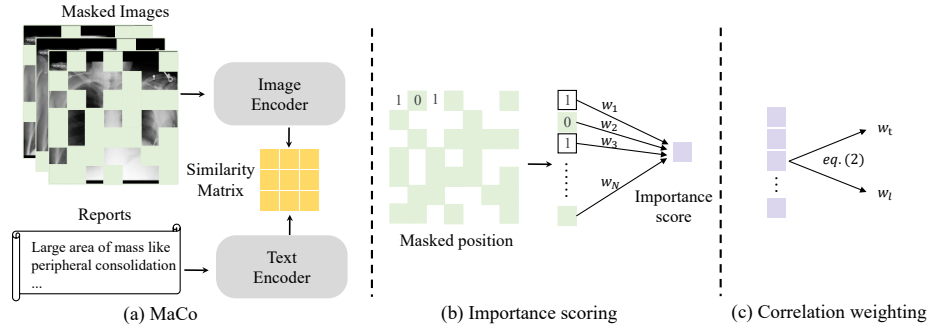


Fig. 2. The details of correlation weighting. We encode masked radiology images and compare them to medical reports using a contrastive loss. The weight of the loss is determined by the mask position at the case-level. We hypothesize that the network can assign a higher weight to the sampled position when it overlaps with common lesion areas.

3.3 Granular Alignment Mechanism

We have established the masked image encoder and report encoder, next, we align the image and text in the feature space to obtain zero-shot capabilities.

Here, we need to address two questions: 1) Can the randomly masked images still correspond to the reports? 2) If there is a correspondence, what is the extent of their correlation? From a clinical expert's perspective, the answer to these two questions depends on the quality of the sampled patches. If the sampled patches can precisely cover the lesion area, the report should be highly correlated. If not, their correlation will be low.

Based on the above observation, we model this process as depicted in Fig. 2(b,c). The motivation behind simulating this process is to score the sampled images based on the relevance masked information. These scores are then used to adjust the temperature in contrastive learning and the weights in the loss function. By doing so, highly correlated paired samples are given a higher weight during the network learning process.

We first reconstructed a binary image of the mask, assigning a value of 0 to the masked regions and a value of 1 to the unmasked regions. We then computed a weighted sum of the mask information for each patch using learnable parameters, resulting in a global representation of the masked regions, as shown in Fig. 2(b).

Subsequently, we derive two weighting coefficients, $w_t \in \mathbb{R}$ and $w_l \in \mathbb{R}$, where w_t serves as the temperature coefficient for the similarity matrix, and w_l is utilized to weight the loss term, as shown in Eq.2.

$$w_t = \exp\left(\frac{\exp(p/\tau_1)}{\sum_d^D \exp(p_d/\tau_1)}\right), \quad (2)$$

$$w_l = \frac{\exp(p/\tau_2)}{\sum_d^D \exp(p_d/\tau_2)}$$

where $p \in \mathbb{R}^{B \times 1}$ represents the batch of embeddings obtained from a fully connected layer for a set of sampled instances. Please note that, as the weight coefficient of the loss function, w_l does not calculate the gradient during training.

Then, we use the weight w_t for the temperature coefficient of the similarity matrix for image's and report's latent space, while using w_l as the contrastive loss function weight for training. Therefore, our contrastive loss can be expressed as:

$$\mathcal{L}_{align} = -w_l \cdot \log\left(\frac{\exp(\langle v, t \rangle / (w_t \cdot \tau_3))}{\sum_k^B \exp(\langle v, t_k \rangle / (w_t \cdot \tau_3))}\right) \quad (3)$$

where $\langle v, t \rangle$ represents the cosine similarity between the masked visual representation $v \in \mathbb{R}^{B \times C}$ and report representation $t \in \mathbb{R}^{B \times C}$. τ_1 and τ_2 are the fixed hyperparameters, parameter τ_3 is a learnable parameter, as stated in [8], respectively.

The final loss function is given by:

$$\mathcal{L} = \lambda \mathcal{L}_{mae} + (1 - \lambda) \mathcal{L}_{align} \quad (4)$$

Here, λ is a hyperparameter used as a scaling factor depending on experiment setting.

4 Experiments

Table 1. Comparison of AUC scores for classification performance on three open-source datasets with varying ratios of annotations. The term 'Epoch' refers to the number of epoch required during training. '*' denotes the MIMIC-CXR re-implement version.

Methods	Epoch	Pretrain-dataset	RSNA			NIH			CheXpert		
			1%	10%	100%	1%	10%	100%	1%	10%	100%
ConVIRT	200	CheXpert	77.4	80.1	81.3	-	-	-	85.9	86.8	87.3
GLoRIA	50	CheXpert	86.1	88.0	88.6	-	-	-	86.6	87.8	88.1
BioViL	30+100PubMed+MIMIC-CXR		88.1	88.4	89.1	-	-	-	-	-	-
ConVIRT*	200	MIMIC-CXR	88.8	91.5	92.7	-	-	-	87.0	88.1	88.1
GLoRIA*	50	MIMIC-CXR	89.7	91.2	92.1	-	-	-	86.5	87.5	87.8
REFERS	45	MIMIC-CXR	89.4	91.6	92.7	76.7	80.9	84.7	87.2	88.1	88.2
MedKLIP	60	MIMIC-CXR	87.3	88.0	89.3	77.2	78.9	83.2	-	-	-
MaCo	30	MIMIC-CXR	91.292.2 93.3 79.083.6 85.5 88.088.2 88.2								

4.1 Datasets

We pretrain MaCo using radiograph and clinical reports release from MIMIC-CXR V2 dataset [21]. We validate the transferability of learned radiograph representations on X-ray based classification and segmentation tasks via end-to-end fine-tuning. Specifically, we evaluate the pre-trained model on 3 X-ray datasets in the classification tasks, which are NIH ChestX-ray [22], CheXpert [23] and RSNA Pneumonia [24]. For the segmentation task, we fine-tune the pre-trained model on SIIM-ACR Pneumothorax [25] dataset. Finally, for the zero-shot phase-grounding, we use MS-CXR [10] to distinguish the range of clinicians annotations from the alignment results.

MIMIC-CXR v2 is a large dataset comprising 377,110 chest x-rays associated with 227,827 imaging studies sourced from the Beth Israel Deaconess Medical Center between 2011 and 2016. During pretraining, we used all paired data, regardless of whether it was frontal or lateral.

CheXpert release a multi-label dataset for chest X-ray classification. To evaluate our model's performance, we follow the official guidelines outlined in [23] and report results for five official selected pathologies. As the official CheXpert test set is not publicly available, we adopt the approach taken by [16] and use the official validation set as our test set. Additionally, following [6], we sample 5,000 images from the official training set to construct our validation set. The resulting training/validation/test split consists of 218,414/5,000/234 images, respectively, representing the entire dataset.

RSNA Pneumonia (RSNA) presents a binary classification problem, where each chest radiograph is classified as either pneumonia or normal. We follow the official data split, which consists of a training set of 25,184 images, a validation set of 1,500 images, and a test set of 3,000 images.

NIH ChestX-ray (NIH) contains 112,120 frontal-view chest radiograph images, and poses a multi-label classification problem for 14 different chest pathologies. The dataset is split into training, validation, and test sets, with each set comprising 70%, 10%, and 20% of the total dataset, respectively.

SIIM-ACR Pneumothorax Segmentation (SIIM) is designed to aid in the development of segmentation models for identifying pneumothorax disease in chest radiographs. The dataset includes over 120,000 frontal-view chest X-rays, each with precise manual segmentation of pneumothorax. To construct the training, validation, and test sets, we follow [9], with each set comprising 70%, 15%, and 15% of the total dataset, respectively.

MS-CXR provide bounding box and sentence pair annotations describing clinical findings visible in a given chest X-ray image. Each sentence describes a single pathology present in the image, and there could be multiple manually annotated bounding boxes corresponding to the description of the single radiological finding. The annotations were collected on a subset of MIMIC-CXR images, which additionally contains labels across eight different pathologies. Totally 1162 annotations across 881 cases were collected, and we utilized the entire dataset to validate the overlap between labeled bounding boxes and the results of vision-language association after pretraining.

4.2 Implement details

For the sake of convenience and comparability, we utilized the widely-used image encoder ViT-B/16 and employed Bert with a width of 768 as our text encoder. We set the training batch size to 512 and used AdamW as the optimizer, with an initial learning rate of 4.5e-4, weight decay of 0.05, β_1 of 0.9, and β_2 of 0.95. In practice, we set the value of λ in Eq. 4 to 0.9, and mini-batch D in Eq. 2 to 16. We set τ_1 and τ_2 to 1 and 16 respectively while initialized the learnable parameter τ_3 to 0.03 according to the experiments.

For finetuning on the segmentation dataset SIIM, we trained the segmentation network using AdamW as the default optimizer, with an initial learning rate of 5e-6, weight decay of 0.05, β_1 of 0.9, and β_2 of 0.999. For finetuning on classification datasets including CheXpert, RSNA Pneumonia and NIH ChestX-ray, we used SGD as the default optimizer with momentum 0.9. We searched for the best learning rate from 8e-3 to 1e-4 to maximize performance on the validation set. For both the pre-training and fine-tuning of the image classification task, we warmed up the network by linearly increasing the learning rate to the set value, and then decreased the learning rate using the cosine decay schedule, following the approach reported in MAE.

4.3 Comparison methods

We begin our analysis by comparing MaCo with a range of pre-training approaches that utilize text as supervision to learn image representations. The baseline comparisons involve: ConVIRT [16], GLoRIA [9], BioViL [10], REFERS [3],

Table 2. Disease-level classification performance on the NIH CHESTX-RAY dataset. The AUC scores are reported under varying ratios of training annotations.

Labeling Ratios		Methods	Average	Atelectasis	Cardiomegaly	Consolidation	Edema	Effusion	Emphysema	Fibrosis	Infiltration	Mass	Nodule	Pleural Thickening	Pneumonia	Pneumothorax	
			76.7	77.5	85.6	78.6	84.9	85.4	79.5	72.3	77.1	67.5	76.2	66.5	71.6	69.3	81.7
1%		REFERS	77.2	-	-	-	-	-	-	-	-	-	-	-	-	-	
		MedKLIP	-	-	-	-	-	-	-	-	-	-	-	-	-	-	
		Model Genesis	70.3	72.1	67.1	75.8	76.1	80.6	72.6	64.8	73.5	65.7	65.2	62.2	67.6	64.8	76.2
		C2L	71.1	75.1	67.1	77.6	75.1	83.4	71.5	66.8	70.0	63.8	70.1	66.2	68.1	65.7	74.4
		Context Restoration	67.8	69.1	64.4	73.2	73.8	78.1	70.0	62.1	70.2	65.2	62.4	59.1	65.0	62.2	73.8
		TransVW	71.3	74.5	68.9	76.7	79.8	81.1	67.9	68.7	68.2	66.8	66.5	66.2	68.5	68.8	75.0
		ImageNet Pre-training	69.8	73.3	69.6	76.0	81.7	80.5	67.1	64.9	64.8	65.8	67.0	62.3	65.7	65.0	74.0
		MaCo	79.4	77.0	91.1	179.3	387.5	587.4	888.2	71.9	85.9	567.8	882.9	967.8	70.3	184.6	
10%		REFERS	80.9	80.1	89.8	79.5	87.8	87.5	88.2	77.2	86.1	69.6	82.0	72.8	74.2	72.2	85.6
		MedKLIP	78.9	-	-	-	-	-	-	-	-	-	-	-	-	-	
		Model Genesis	76.0	77.2	72.8	77.5	85.7	85.2	81.0	75.3	78.0	68.4	73.1	69.5	72.2	67.7	80.4
		C3L	76.6	78.0	75.5	77.5	84.1	85.7	81.2	73.7	79.5	67.4	77.5	71.7	72.0	67.3	81.9
		Context Restoration	73.8	75.5	70.6	77.1	84.5	84.2	79.4	73.1	67.5	68.1	70.9	66.9	71.7	65.2	79.1
		TransVW	74.4	76.5	70.8	77.6	83.0	84.8	79.7	69.9	74.7	68.5	72.1	68.3	72.4	63.2	79.6
		ImageNet Pre-training	74.4	74.2	79.8	75.9	85.7	83.2	80.4	72.1	74.0	64.1	71.7	65.6	69.6	66.2	79.7
		MaCo	83.681.991.580.889.388.592.083.592.270.485.974.177.475.287.1														
100%		REFERS	84.7	83.0	92.3	82.1	90.2	88.7	91.4	83.9	93.3	74.1	85.5	76.7	78.5	77.0	89.1
		MedKLIP	83.2	-	-	-	-	-	-	-	-	-	-	-	-	-	
		Model Genesis	81.0	78.8	84.5	79.2	87.8	86.6	89.7	81.0	85.2	71.1	81.9	73.2	75.8	73.0	85.6
		C4L	82.2	81.1	90.2	81.0	88.1	88.0	88.3	80.8	86.8	72.0	82.7	74.1	76.2	75.3	85.9
		Context Restoration	78.7	75.8	82.9	76.4	86.6	84.8	88.2	78.6	83.0	70.0	79.6	69.5	73.2	69.4	84.0
		TransVW	81.7	79.8	85.0	80.0	88.2	87.1	90.1	81.8	85.9	72.3	82.6	74.4	76.6	74.0	86.1
		ImageNet Pre-training	80.0	78.3	89.3	77.6	87.9	85.9	87.4	78.5	88.8	65.9	79.9	70.7	74.5	71.0	84.7
		MaCo	85.583.892.982.390.789.393.985.893.5	72.0	87.277.580.078.189.3												

MGCA [19], Med-UniC [26], M3AE [27], Med-KLIP [2], and MRM [6]. Specifically, ConVIRT proposes to learn medical visual representations by contrasting paired radiographs and sentences from radiology reports. GLoRIA improves upon ConVIRT by contrasting radiograph patches and words in the reports. BioViL and REFERS incorporate masked language modeling loss into contrastive learning, with REFERS introducing a multi-view fusion attention mechanism to better align the representations of each radiograph and its associated report. M3AE employs mask modeling in both the image and language modalities to investigate the performance of pre-trained models on natural datasets. MedKlip utilizes a report filter to extract medical entities and employs a more complex modal fusion module to aggregate features, while MRM leverages a masking mechanism similar to M3AE and has achieved the most advanced results in the medical field.

In addition, to compare our method with a wider range of approaches, we also introduce some image-based self-supervision methods in our analysis. Including Context Restoration [28], Model Genesis [29], TransVW [30], C2L [31] and ImageNet pre-training [22].

Subsequently, we presented zero-shot phase-grounding results and compared them with the most relevant methods of GLoRIA and BioViL. It should be

noted that Medklip is unable to handle free-form text, while MRM and M3AE are unable to obtain the zero-shot results due to their training strategy. Finally, we demonstrated the weight visualization of the proposed masked contrastive interaction mechanism, which uses attention maps to indicate that our approach weights the masked image representations in an understandable manner.

4.4 Results

To validate the effectiveness of MaCo as a zero-shot foundational model in down-stream annotation tasks, we begin by comparing its performance on fine-tuning tasks. This includes segmentation and classification tasks with varying annotation ratios. Subsequently, we provide qualitative and quantitative evidence of MaCo’s zero-shot phase grounding capabilities. Additionally, we conduct a comparative analysis with non-zero-shot methods to highlight subtle differences in performance on down-stream tasks. Finally, we present visualizations of the proposed weighted mechanism to demonstrate how our network accurately learns relevant regions.

Comparison of label-efficient classification We present the finetuning results of the foundation models on classification tasks using the CheXpert, RSNA Pneumonia, and NIH CHEST X-RAY datasets. In particular, we evaluate the performance of different annotation ratios and compare them with the currently prevailing contrast learning methods.

To begin with, we compare the results of model pretraining on different datasets, specifically pretraining ConVIRT and GLoRIA on CheXpert and MIMIC-CXR, respectively, as shown in Table 1. Through a comparison of ConVIRT and GLoRIA’s performance on the CheXpert and MIMIC-CXR datasets, we observed that models trained on the MIMIC-CXR dataset achieved superior results. This could be attributed to the larger dataset size of MIMIC-CXR (377,110 images) compared to CheXpert (191,229 images), which is particularly beneficial for contrastive learning methods [8]. Notably, MaCo consistently outperformed other contrastive-based methods across various datasets and annotation proportions. This can be attributed to MaCo’s integration of pretext task in the image branch, resulting in improved image features. Furthermore, we compared the number of epochs required for pre-training, which serves as an indicator of the method’s effectiveness in learning robust features, especially when dealing with large-scale datasets where an excessive number of epochs might be impractical. Remarkably, MaCo achieves training completion in only 30 epochs, significantly reducing the training time compared to alternative methods.

In Table 2, we compare the performance of MaCo on disease-level classification in the NIH ChestX-ray dataset. Here, we introduce some image-based pretext task methods to validate our method in a wider range. Since MedKLIP did not provide more detailed category results, we only reported its average AUC. The utilization of medical reports in MedKLIP has resulted in higher performance compared to methods that rely solely on image-based information. This

confirms the effectiveness of incorporating medical reports in pre-training models. In comparison, MaCo outperformed MedKLIP with AUC scores of 79.4% vs 77.2%, 83.6% vs 78.9%, and 85.5% vs 83.2% at annotation ratios of 1%, 10% and 100% respectively.

Overall, compared to currently popular algorithms, MaCo achieved the best performance on the three open-source classification datasets, regardless of the annotation ratio used. Promising results have been observed, indicating the effectiveness of the proposed method for fine-tuning classification tasks.

Comparison of label-efficient segmentation We also compared the segmentation results obtained through finetuning with 1%, 10% and 100% annotations data. We conducted experiments on SIIM dataset, and compared our approach with state-of-the-art methods, including ConVIRT, GLoRIA, MGCA, Med-UniC, as shown in Table 3.

Table 3. Comparison of Dice scores for segmentation performance on SIIM with varying ratios of annotations.

Methods	1%	10%	100%
ConVIRT	25.0	43.2	59.9
GLoRIA	35.8	46.9	63.4
MGCA	49.7	59.3	64.2
Med-UniC	56.7	62.2	64.4
MaCo	58.8	70.7	89.6

Our method consistently outperformed other approaches in all experiments. Specifically, the results indicate that MaCo achieves comparable performance to the current state-of-the-art method, Med-UniC, at a low annotation rate of 1%. As the annotation ratio increased, MaCo demonstrated significant improvements in performance. At a 10% annotation ratio, MaCo achieved a notable boost with a performance of 70.7% compared to Med-UniC’s 62.2%. This highlights MaCo’s ability to capitalize on additional labeled data to enhance its feature representation and segmentation accuracy.

The above experiments demonstrate the advantages of MaCo in terms of segmentation performance gains with increasing levels of annotation, showcasing its potential for reducing the reliance on manual labeling and improving the efficiency of medical data analysis.

Comparison of zero-shot phase grounding Interpretable visualization of the correlations between modalities is necessary to establish clinical trust and remove barriers to adoption. We evaluated the zero-shot phase grounding performance of MaCo on the MS-CXR dataset, which provides medical freely sentences and corresponding bounding boxes. Notably, thanks to the proposed variable alignment module, we were able to utilize the weight map shown in Fig.

Table 4. Comparison of classification performance with state-of-the-art non-contrastive learning methods, taking into consideration their trade-off in sacrificing the capability of zero-shot learning.

Methods	Zero-shot	RSNA			NIH		
		1%	10%	100%	1%	10%	100%
M3AE	w/o	89.0	90.8	92.3	-	-	-
MRM	w/o	91.3	92.7	93.3	79.4	84.0	85.9
MaCo	w	91.2	92.2	93.3	79.4	83.6	85.5

4. We first applied the softmax function along the pixels dimension (denoting the related patch weight) of the final weight map, with a soft threshold τ . We then multiplied the resulting weights with the patch-based similarity matrices computed from the image modalities. Finally, the latent features of images and reports was calculated to obtain mIoU and CNR.

Table 5. Comparison of zero-shot phase grounding for segmentation performance on MS-CXR datasets.

Methods	mIoU	CNR
ConVIRT	0.238	0.818
GLoRIA	0.246	0.930
BioViL	0.266	1.027
MaCo	0.268	1.152

In Table 4, we compared the phase grounding performance with methods, including ConVIRT, GLoRIA, and BioViL. As the first method in the medical field to achieve zero-shot capability using discriminative approaches, ConVIRT achieved an mIoU of 0.238 and a CNR score of 0.818. Among the other methods, BioViL achieved higher metrics with an mIoU of 0.266 and a CNR of 1.027, likely benefiting from the word-weighting approach proposed in GLoRIA and using a larger pretrained dataset. In comparison, MaCo obtained the highest scores with an mIoU of 0.268 and a CNR of 1.152. This could be attributed to the fine-grained alignment achieved by the interaction of mask autoencoder and contrastive learning.

The qualitative results are presented in Fig. 3, where each row represents an instance’s visual-textual correlation heatmap obtained from different methods. We showcase examples of diseases from different anatomical regions, including cardiomegaly, opacity, and atelectasis. In the first row, GLoRIA and BioViL only partially capture the extent of the diseases, while MaCo extracts more complete regions. In the second row, we demonstrate cases with multiple lesions. Here, BioViL can only uncover information from one of the lesions, whereas MaCo and GLoRIA both exhibit relevance to the text in both dashed boxes, with MaCo displaying a more comprehensive representation.

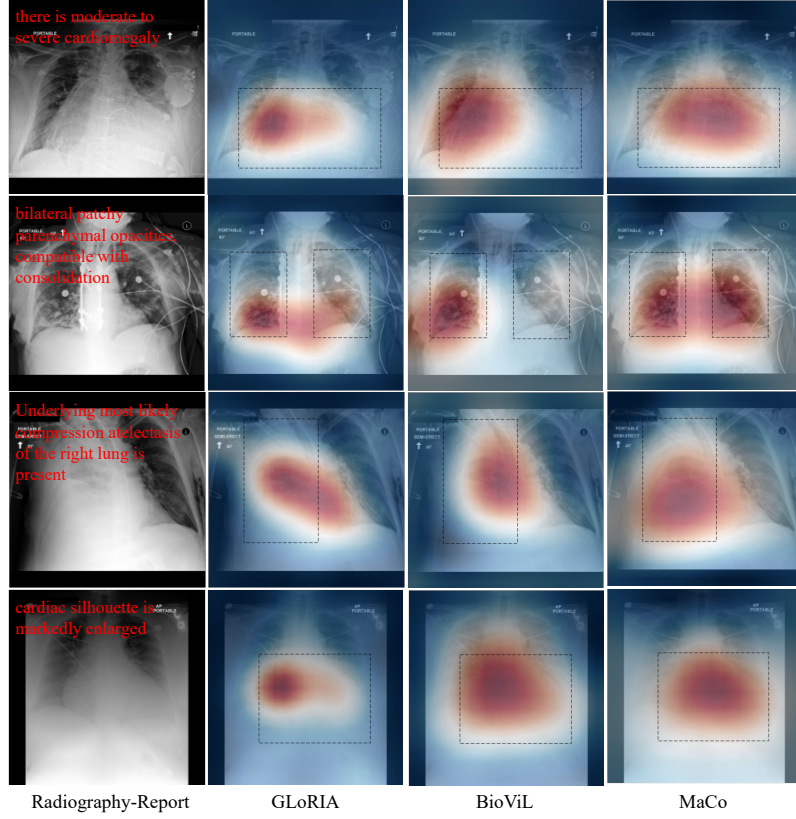


Fig. 3. Phase grounding with free-text. We visualize the association of vision and language on the MS-CXR dataset. In the first column, the free-text annotations are marked in red font, while the gold standard annotations outlined by clinical experts are represented with dashed boxes. We compared the results obtained from GLoRIA and BioViL.

The above results demonstrate the performance of MaCo in zero-shot phase grounding. In terms of quantitative metrics, we compared it with three popular methods and achieved comparable performance. In the quantitative results, we showcased superior textual-visual correlation, whether in the completeness of multi-lesion regions or in single-region cases. MaCo exhibited better performance in terms of capturing the textual-visual associations.

Comparison with methods without zero-shot capability We consider zero-shot capability as a crucial skill in clinical settings, as it extends task generalization and enables the demonstration of learned visual-language associations in phase grounding, thereby fostering trust among clinical practitioners.

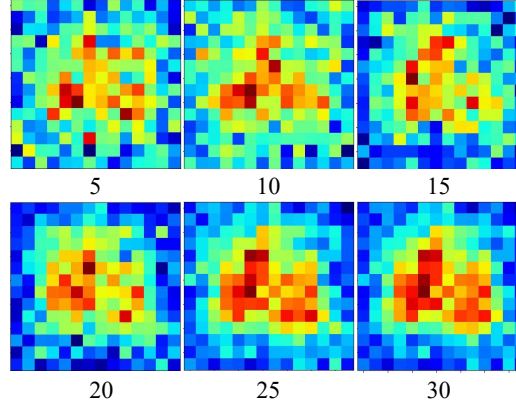


Fig. 4. Linear weight of the proposed variable fine-grain alignment. The number under the picture indicates the training epoch. After training, the linear weights are larger in regions with a higher incidence of disease and smaller in the background regions around the edges.

Nevertheless, we conducted a comparative analysis between MaCo and several methods lacking zero-shot capability to obtain a more objective evaluation.

Table 6. Comparison of phase grounding and classification performance between the proposed MaCo and baseline methods.

Methods	MS-CXR			RSNA		
	mIoU	CNR	PG	1%	10%	100%
MAE	-	-	-	81.3	82.1	91.2
+CLIP	0.211	0.928	0.366	90.9	92.1	93.0
+Interaction Weighted	0.268	1.152	0.429	91.2	92.2	93.3

We conducted a comparative analysis of the classification performance among methods lacking zero-shot capability including M3AE and MRM, as shown in Table 5. MRM adopt both masked recovery and super-resolution as the pretext task, achieved the highest performance and appears to surpass current contrastive learning based methods. However, in order to achieve the high performance, MRM and M3AE sacrifices the zero-shot and text-image explainability and visualization, potentially reducing its scalability and practicality. Nevertheless, MaCo still achieves performance comparable to MRM, with the capabilities of zero-shot and visualization. The slight performance gap towards MRM may be compensated for in the future by the continuous increase of clinical daily examine data, as larger datasets have been shown to have a more significant impact on contrastive learning [8, 11].

Visualization of Granular Alignment Mechanism To demonstrate the effectiveness of MaCo in the interaction between masking and contrastive learning, we visualize the linear weights proposed in Section 3.3, as shown in Fig. 4. Each pixel represents the corresponding weight of an image patch. Initially, during the training stage, the weights are dispersed without prominent positions, indicating that the network hasn't learned the distinctions between different patches. As the training epochs increase, the weights in the central region of the image (typically the location of the lungs) gradually increase, while the weights in the background regions decrease. This indicates that the model assigns greater importance to image patches near the lungs, considering them to contain more informative content compared to the background regions. The weight map not only visualizes the model's attention on different patch positions but also has the potential to enhance down-stream task performance, as demonstrated in the following analysis.

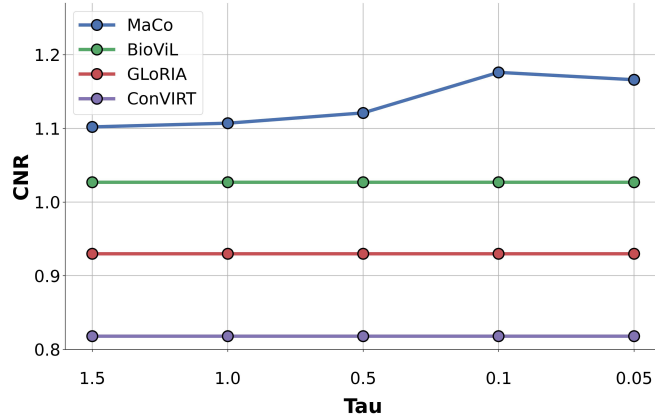


Fig. 5. Zero-shot segmentation performance on MS dataset. We plotted score curves for different τ (Tau) values. The peak values of MaCo's mIoU and CNR were achieved at $\tau = 0.02$ and 0.01 , respectively.

In Fig. 5, we illustrate the variation of mIoU and CNR scores with different τ values when multiply to the logits during testing, as mentioned in section 1.1.3. Since other methods do not have this interaction mechanism, their indicators will not change with τ . The best-performing τ value was determined to be 0.1, resulting in an mIoU score of 0.268 and an CNR score of 1.152. In comparison, BioViL achieved an mIoU score of 0.266 and an CNR score of 1.027.

Effectiveness of granular alignment and weighting mechanism In this section, we compare our proposed method to the baseline approach to highlight the effectiveness through classification and phase grounding, as shown in Table 6.

We initially selected the MAE trained solely on the image modality as our baseline model. Since MAE lacks the ability to interact with reports, the grounding capabilities is limited. MAE achieved AUC of 81.3% on the RSNA dataset with 1% annotations. We then incorporated CLIP into MAE (denote as +CLIP) to achieve granular alignment. By leveraging contrastive learning, we gained zero-shot capabilities and achieved an mIoU of 0.211 in the grounding task on the MS-CXR dataset. Additionally, we observed improvements in the classification task, indicating that the inclusion of expert knowledge from medical reports can enhance the model’s performance.

Finally, we introduced the correlation weighting mechanism. Higher results were observed, particularly in phase grounding, where there was a significant improvement in mIoU (0.268 vs. 0.211). This suggests that the model’s feature representation capabilities were enhanced by incorporating the relevance weighting mechanism.

5 Conclusion

Fine-grained knowledge understanding and limited annotation present significant challenges in the development of medical foundation models. In this paper, we propose MaCo, a novel approach that addresses these challenges by focusing on achieving granular alignment between radiography and reports to obtain fine-grained representation.

We evaluate the effectiveness of our method on six open-source datasets, including label-efficient classification and segmentation tasks, with seven state-of-the-art comparison methods. Additionally, we demonstrated our zero-shot ability on the phase-grounding task, and clearly demonstrated the comparison of qualitative and quantitative indicators with other most advanced methods. Furthermore, we quantify the degree of correlation between each radiograph patch’s location and its corresponding report, thereby highlighting the model’s capability to effectively discriminate regions of reports always focused on.

We also observed some interesting phenomena in the experiment. Based on the pre-training data of MIMIC-CXR, the method of coupled radiography and reports seems to achieve higher down-stream task performance. We hypothesize that these methods may prioritize complementary features from two modalities. However, this comes at the cost of sacrificing zero-shot capability and related visualizations, which can impede their applicability in diverse clinical environments and establishing trust among medical professionals. Fortunately, the slight performance decrease of MaCo in classification tasks may be compensated by a more extensive dataset, as contrastive learning has been shown to have more advantages in large datasets [8, 11, 16, 32].

In conclusion, this paper introduces MaCo, a novel medical foundation model, aimed at addressing the challenges of fine-grained knowledge understanding and limited annotation in the medical domain. By incorporating granular alignment, MaCo takes the benefits of pretext tasks and contrastive learning. The promis-

ing results obtained from fine-tuning and zero-shot generalization experiments underscore the potential of MaCo in advancing medical foundation models.

6 Acknowledgments

This research was partly supported by the National Natural Science Foundation of China (62222118, U22A2040), Shenzhen Science and Technology Program (RCYX20210706092104034, JCYJ20220531100213029), Guangdong Provincial Key Laboratory of Artificial Intelligence in Medical Image Analysis and Application (2022B1212010011), the major key project of Peng Cheng Laboratory under grant PCL2023AS1-2, and Key Laboratory for Magnetic Resonance and Multimodality Imaging of Guangdong Province (2020B1212060051).

References

1. Pranav Rajpurkar and Matthew P Lungren. The current and future state of ai interpretation of medical images. *New England Journal of Medicine*, 388(21):1981–1990, 2023.
2. Chaoyi Wu, Xiaoman Zhang, Ya Zhang, Yanfeng Wang, and Weidi Xie. Medklip: Medical knowledge enhanced language-image pre-training. *medRxiv*, pages 2023–01, 2023.
3. Hong-Yu Zhou, Xiaoyu Chen, Yinghao Zhang, Ruibang Luo, Liansheng Wang, and Yizhou Yu. Generalized radiograph representation learning via cross-supervision between images and free-text radiology reports. *Nature Machine Intelligence*, 4(1):32–40, jan 2022.
4. Kaiming He, Xinlei Chen, Saining Xie, Yanghao Li, Piotr Dollár, and Ross Girshick. Masked autoencoders are scalable vision learners. In *2022 IEEE/CVF Conference on Computer Vision and Pattern Recognition (CVPR)*, pages 15979–15988, 2022.
5. Xiaoman Zhang, Chaoyi Wu, Ya Zhang, Weidi Xie, and Yanfeng Wang. Knowledge-enhanced visual-language pre-training on chest radiology images. *Nature Communications*, 14(1):4542, 2023.
6. Hong-Yu Zhou, Chenyu Lian, Liansheng Wang, and Yizhou Yu. Advancing radiograph representation learning with masked record modeling. *arXiv preprint arXiv:2301.13155*, 2023.
7. Zhihong Chen, Yuhao Du, Jinpeng Hu, Yang Liu, Guanbin Li, Xiang Wan, and Tsung-Hui Chang. Multi-modal masked autoencoders for medical vision-and-language pre-training. In *International Conference on Medical Image Computing and Computer-Assisted Intervention*, pages 679–689. Springer, 2022.
8. Alec Radford, Jong Wook Kim, Chris Hallacy, Aditya Ramesh, Gabriel Goh, Sandhini Agarwal, Girish Sastry, Amanda Askell, Pamela Mishkin, Jack Clark, et al. Learning transferable visual models from natural language supervision. In *International conference on machine learning*, pages 8748–8763. PMLR, 2021.
9. Shih-Cheng Huang, Liyue Shen, Matthew P. Lungren, and Serena Yeung. Gloria: A multimodal global-local representation learning framework for label-efficient medical image recognition. In *2021 IEEE/CVF International Conference on Computer Vision (ICCV)*, pages 3922–3931, 2021.
10. Benedikt Boecking, Naoto Usuyama, Shruthi Bannur, Daniel C Castro, Anton Schwaighofer, Stephanie Hyland, Maria Wetscherek, Tristan Naumann, Aditya Nori, Javier Alvarez-Valle, et al. Making the most of text semantics to improve biomedical vision–language processing. In *European conference on computer vision*, pages 1–21. Springer, 2022.
11. Andrew Ng and Michael Jordan. On discriminative vs. generative classifiers: A comparison of logistic regression and naive bayes. *Advances in neural information processing systems*, 14, 2001.
12. Ishan Misra and Laurens van der Maaten. Self-supervised learning of pretext-invariant representations. In *Proceedings of the IEEE/CVF conference on computer vision and pattern recognition*, pages 6707–6717, 2020.
13. Saleh Albelwi. Survey on self-supervised learning: auxiliary pretext tasks and contrastive learning methods in imaging. *Entropy*, 24(4):551, 2022.
14. Ashish Jaiswal, Ashwin Ramesh Babu, Mohammad Zaki Zadeh, Debapriya Banerjee, and Fillia Makedon. A survey on contrastive self-supervised learning. *Technologies*, 9(1):2, 2020.

15. Yuan Jin, Wray Buntine, Francois Petitjean, and Geoffrey I Webb. Discriminative, generative and self-supervised approaches for target-agnostic learning. *arXiv preprint arXiv:2011.06428*, 2020.
16. Yuhao Zhang, Hang Jiang, Yasuhide Miura, Christopher D Manning, and Curtis P Langlotz. Contrastive learning of medical visual representations from paired images and text. In *Machine Learning for Healthcare Conference*, pages 2–25. PMLR, 2022.
17. Zifeng Wang, Zhenbang Wu, Dinesh Agarwal, and Jimeng Sun. Medclip: Contrastive learning from unpaired medical images and text. In *Proceedings of the 2022 Conference on Empirical Methods in Natural Language Processing*, pages 3876–3887, 2022.
18. Shruthi Bannur, Stephanie Hyland, Qianchu Liu, Fernando Perez-Garcia, Maximilian Ilse, Daniel C Castro, Benedikt Boecking, Harshita Sharma, Kenza Bouzid, Anja Thieme, et al. Learning to exploit temporal structure for biomedical vision-language processing. In *Proceedings of the IEEE/CVF Conference on Computer Vision and Pattern Recognition*, pages 15016–15027, 2023.
19. Fuying Wang, Yuyin Zhou, Shujun Wang, Varut Vardhanabhuti, and Lequan Yu. Multi-granularity cross-modal alignment for generalized medical visual representation learning. *Advances in Neural Information Processing Systems*, 35:33536–33549, 2022.
20. Jacob Devlin, Ming-Wei Chang, Kenton Lee, and Kristina Toutanova. Bert: Pre-training of deep bidirectional transformers for language understanding. *arXiv preprint arXiv:1810.04805*, 2018.
21. Alistair EW Johnson, Tom J Pollard, Nathaniel R Greenbaum, Matthew P Lungren, Chih-ying Deng, Yifan Peng, Zhiyong Lu, Roger G Mark, Seth J Berkowitz, and Steven Horng. Mimic-cxr-jpg, a large publicly available database of labeled chest radiographs. *arXiv preprint arXiv:1901.07042*, 2019.
22. Xiaosong Wang, Yifan Peng, Le Lu, Zhiyong Lu, Mohammadhadi Bagheri, and Ronald M Summers. Chestx-ray8: Hospital-scale chest x-ray database and benchmarks on weakly-supervised classification and localization of common thorax diseases. In *Proceedings of the IEEE conference on computer vision and pattern recognition*, pages 2097–2106, 2017.
23. Jeremy Irvin, Pranav Rajpurkar, Michael Ko, Yifan Yu, Silviana Ciurea-Ilcus, Chris Chute, Henrik Marklund, Behzad Haghgoo, Robyn Ball, Katie Shpanskaya, et al. Chexpert: A large chest radiograph dataset with uncertainty labels and expert comparison. In *Proceedings of the AAAI conference on artificial intelligence*, volume 33, pages 590–597, 2019.
24. George Shih, Carol C Wu, Safwan S Halabi, Marc D Kohli, Luciano M Prevedello, Tessa S Cook, Arjun Sharma, Judith K Amorosa, Veronica Arteaga, Maya Galperin-Aizenberg, et al. Augmenting the national institutes of health chest radiograph dataset with expert annotations of possible pneumonia. *Radiology: Artificial Intelligence*, 1(1):e180041, 2019.
25. American College of Radiology, American Association of Physicists in Medicine (AAPM), et al. Society for imaging informatics in medicine (siim). *Practice guideline for digital radiography (Resolution 42, adopted in 2007)[visionato il 4 dicembre 2012]. Disponibile su: www. siimweb. org*, 2014.
26. Zhongwei Wan, Che Liu, Mi Zhang, Jie Fu, Benyou Wang, Sibo Cheng, Lei Ma, César Quilodrán-Casas, and Rossella Arcucci. Med-unic: Unifying cross-lingual medical vision-language pre-training by diminishing bias. *arXiv preprint arXiv:2305.19894*, 2023.

27. Xinyang Geng, Hao Liu, Lisa Lee, Dale Schuurmans, Sergey Levine, and Pieter Abbeel. Multimodal masked autoencoders learn transferable representations. *arXiv preprint arXiv:2205.14204*, 2022.
28. Liang Chen, Paul Bentley, Kensaku Mori, Kazunari Misawa, Michitaka Fujiwara, and Daniel Rueckert. Self-supervised learning for medical image analysis using image context restoration. *Medical image analysis*, 58:101539, 2019.
29. Zongwei Zhou, Vatsal Sodha, Jiaxuan Pang, Michael B Gotway, and Jianming Liang. Models genesis. *Medical image analysis*, 67:101840, 2021.
30. Fatemeh Haghghi, Mohammad Reza Hosseinzadeh Taher, Zongwei Zhou, Michael B Gotway, and Jianming Liang. Transferable visual words: Exploiting the semantics of anatomical patterns for self-supervised learning. *IEEE transactions on medical imaging*, 40(10):2857–2868, 2021.
31. Hong-Yu Zhou, Shuang Yu, Cheng Bian, Yifan Hu, Kai Ma, and Yefeng Zheng. Comparing to learn: Surpassing imagenet pretraining on radiographs by comparing image representations. In *Medical Image Computing and Computer Assisted Intervention–MICCAI 2020: 23rd International Conference, Lima, Peru, October 4–8, 2020, Proceedings, Part I 23*, pages 398–407. Springer, 2020.
32. Rajat Raina, Yirong Shen, Andrew Mccallum, and Andrew Ng. Classification with hybrid generative/discriminative models. *Advances in neural information processing systems*, 16, 2003.